Bimodal size distribution of self-assembled $In_xGa_{1-x}As$ quantum dots

S. Anders, C. S. Kim, B. Klein, Mark W. Keller, and R. P. Mirin

National Institute of Standards and Technology, Boulder, Colorado 80305

A. G. Norman

National Renewable Energy Laboratory, Golden, Colorado 80401

We investigate quantization of energy levels in self-assembled $In_xGa_{1-x}As$ quantum dots that are embedded in a GaAs matrix. We use capacitance and photoluminescence spectroscopies to analyze the evolution of the energy levels with varying amounts of deposited $In_xGa_{1-x}As$. These techniques suggest that the size distribution of the quantum dots contains two well-separated peaks. Transmission electron microscopy confirms a bimodal size distribution and further shows that the big and the small quantum dots have different shapes. In addition, we use an effective-mass based method to calculate the lowest energy states of quantum dots with the physical dimensions obtained by transmission electron and atomic force microscopies. Our results allow us to construct the energy-level diagrams of the two kinds of quantum dots.

The strong quantization of the energy levels of self-assembled semiconductor quantum dots (QDs), a manifestation of their nanoscale size, can be utilized for optoelectronic applications such as QD lasers[1,2] and charge-storage devices.[3,4] From a fundamental point of view, charge carriers populating semiconductor QDs can be considered as model systems for quantum-mechanical interactions between confined electrons and holes.[5,6] The self-assembly process poses interesting questions regarding the growth dynamics of the QDs and the resulting distribution of sizes and shapes.[7–10] For example, it has been found that certain growth conditions result in a bimodal or even multimodal[11,12] QD size distribution. In previous work, bimodal QD systems have been investigated with atomic force microscopy (AFM)[13–19] and photoluminescence (PL) spectroscopy.[16,19,20]

In this report, we combine PL and capacitance spectroscopies at liquid He temperature, atomic force microscopy (AFM) and transmission electron microscopy (TEM), and effective-mass based calculations to obtain a complete picture of the evolution of the energy levels in the QDs with varying $In_xGa_{1-x}As$ coverage. The PL and capacitance measurements show that two distinct sets of QDs with well-separated energy levels coexist in the sample. The TEM and AFM not only measure the average sizes of the two kinds of QDs, but also show that the shapes of the big and small QDs are different. Combining these measurements with our calculations, we construct a consistent picture for the energy-level diagrams of both kinds of QDs and also speculate about the growth dynamics that give rise to the bimodal size distribution.

The samples for capacitance and PL spectroscopies were grown by molecular beam epitaxy on a semi-insulating (100) GaAs substrate. The epilayers consisted of a buried contact layer of 200 nm GaAs (n type, 4×10^{18} cm^{-3}), a 45 nm undoped GaAs tunnel barrier, the $In_xGa_{1-x}As$ QDs, 30 nm of undoped GaAs, 59 periods of a (3 nm AlAs/1 nm GaAs) blocking barrier, and 5 nm of GaAs. The QDs were deposited at a substrate temperature of 530 °C. In and Ga were deposited with no As in order to enhance the surface migration.

Nine cycles of the following deposition were used to form the QDs: 0.25 monolayers of In, 5 s of As$_2$, 0.31 monolayers of Ga, and 5 s of As$_2$. The total amount of deposited $In_{0.44}Ga_{0.56}As$ was 5.0 monolayers. The sample for AFM and TEM was grown in a similar fashion, except that the growth ended immediately after the QDs were deposited.

In order to analyze the evolution of QD size and shape with increasing $In_xGa_{1-x}As$ coverage, the wafer was not rotated during growth. Because of the position of the In cell with respect to the wafer, this resulted in a gradient of deposited $In_xGa_{1-x}As$ such that the change in $In_xGa_{1-x}As$ coverage across the part of the wafer for which we show results is 0.3 monolayers (assuming a point In source and a $1/R^2$ decrease of the In flux).

To process our sample for capacitance spectroscopy, we wet-etched 100 nm deep, so that only 35 periods of superlattice remained, and sputtered 100 nm SiO$_2$ as an insulating layer. This increased the yield of the samples by preventing a low turn-on voltage of the structure, which was probably caused by Au from the top contact diffusing into the sample. We have confirmed that our results were not affected by this procedure, using samples from the same wafer but without etching and SiO$_2$, for comparison.

The narrow size distribution of self-assembled QDs makes it possible to investigate their properties on an ensemble of millions of QDs. The signal will be broadened by the distribution of sizes, but it will also be amplified by the large number of QDs. The result is that features originating from individual energy levels of the QDs are readily observable using techniques such as PL and capacitance spectroscopies. For capacitance spectroscopy, the QDs were sandwiched between an insulating blocking layer and a tunnel barrier consisting of undoped GaAs (Fig. 1, inset). Ohmic contact to the n-doped layer underneath the tunnel barrier was achieved by annealing AuGe. We placed a pad of Au with an area of 1 mm^2 above the blocking layer. The energetic position of the energy levels in the QDs with respect to the conduction-band edge in the n-doped layer can be varied by applying a dc voltage across the QDs. Using the
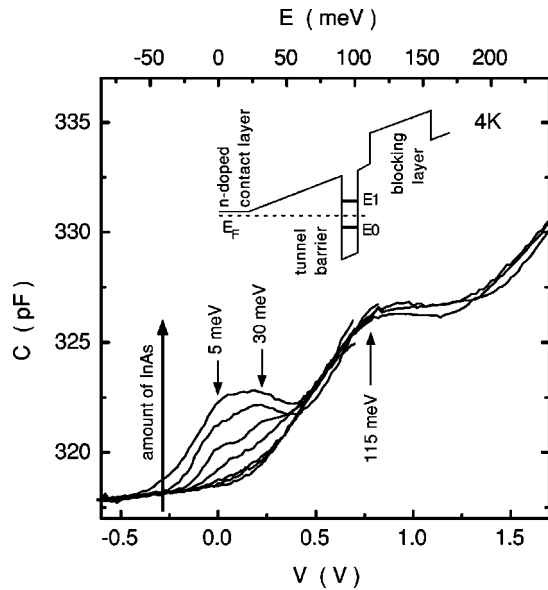
FIG. 1. Capacitance spectra measured at seven different positions on the wafer, i.e., at different amounts of deposited $In_xGa_{1-x}As$. The positions are spaced evenly by 1.5 mm. The voltage is converted to an energy scale by using a lever arm of 7. Inset: Conduction-band diagram of the structure.
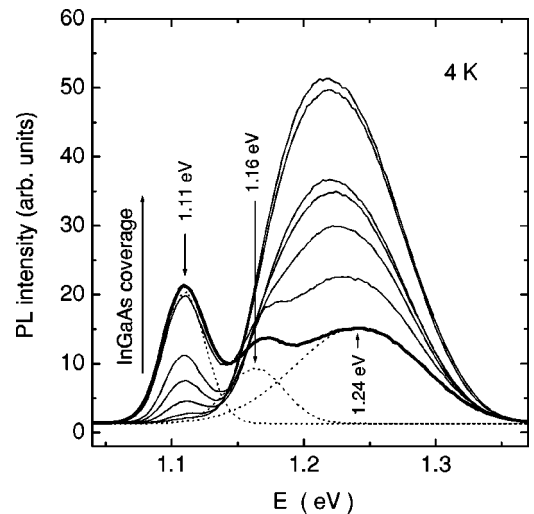

FIG. 2. Photoluminescence spectra at the same seven positions on the wafer as for the data in Fig. 1. Dotted line: Gaussian fit to the bold trace, which corresponds to the highest amount of deposited $In_xGa_{1-x}As$.

lever-arm argument (i.e., regarding the structure as a voltage divider) with a lever of 7.0 for the sample presented here, we can convert an applied voltage into a shift in energy.[21] When an energy level in the QDs lines up with the conduction-band edge in the n-doped layer, electrons can tunnel on and off the QDs, which causes an increase in the capacitance of the structure. We monitored the capacitance at a temperature of 4 K using a lock-in amplifier with an ac excitation of 10 mV and a frequency of typically 100 Hz. The capacitance is proportional to the density of states in the QDs,[21] and a trace of capacitance vs voltage allows us to obtain the energetic difference between electron states in the QD.

PL spectroscopy serves as a complementary tool, since it detects the energetic difference between electron and hole states with the same quantum number. PL measurements were made at 4 K by focusing the 514.5 nm line of an Ar^+ laser onto the sample. The spot size on the sample was approximately $(100 \ \mu m)^2$. The photoexcited electrons and holes diffuse into the QDs, relax to the lowest available states, and recombine. The emitted light was focused on the input slit of a 0.85 m monochromator and detected as a function of wavelength with a liquid-nitrogen-cooled $In_xGa_{1-x}As$ detector and a lock-in amplifier.

The capacitance spectroscopy data in Fig. 1 show three peaks at energies 5, 30, and 115 meV, corresponding to three energy levels in the QDs. (We have confirmed on several samples that the peaks at 5 and 30 meV are indeed two separate peaks). The peaks are located on top of a monotonically increasing background capacitance. The data were taken at seven different positions on the wafer that were separated by 1.5 mm. We might expect that the gradient in the $In_xGa_{1-x}As$ coverage results in a gradient in the mean size or the density of the QDs across the seven positions on the wafer. However, the capacitance spectroscopy data in

Fig. 1 cannot be explained by a gradient either in the size or density of the QDs. If the seven traces were taken at positions that differ in QD density, all of the features would become less pronounced as the QD density decreases. If the QDs were to grow bigger as more $In_xGa_{1-x}As$ is deposited, we would observe a redshift of the features, since the energy levels in big QDs are lower.[22] Surprisingly, we found that the capacitance peak at 115 meV depended very little on the amount of deposited $In_xGa_{1-x}As$ whereas the peaks at 5 meV and 30 meV disappeared as less $In_xGa_{1-x}As$ was deposited.

In Fig. 2, PL spectroscopy also showed that the first two peaks, here located at 1.11 eV and 1.16 eV, disappeared as less $In_xGa_{1-x}As$ is deposited. The third peak, at 1.24 eV, grew as the lower two peaks disappeared, because the electrons and holes that were photoexcited by the Ar^+ laser can now exclusively populate the states that cause the third peak. We note that for the same reason, i.e., states competing for excited electron-hole pairs, the $In_xGa_{1-x}As$ wetting layer peak (measured at about 1.34 eV on similar samples), was absent in this plot.

The combined PL and capacitance data suggest that for large amounts of deposited $In_xGa_{1-x}As$, two sets of QDs coexist on the sample. Accordingly, two sets of signals were observed. As less $In_xGa_{1-x}As$ is deposited, one set of QDs disappears.

The position of the energy levels in the QDs is not only influenced by their size,[22] but also by strain,[23] In content,[24,25] and shape.[26,27] In general, these parameters are codependent; for example, larger coherent QDs exhibit more strain. The size and to some extent the shape of the QDs can be obtained by TEM and AFM imaging. The upper panel of Fig. 3, a suppressed diffraction bright field image[28] taken as close as possible to zero defocus to minimize the effects of strain on the image, shows the mass and thickness contrast of $In_xGa_{1-x}As$ QDs on a GaAs surface. These QDs were grown under the same conditions as the QDs for the PL and capacitance spectroscopies, except that, to facilitate the TEM im-
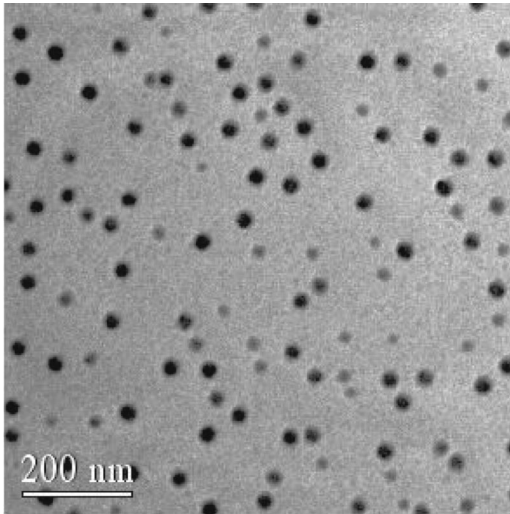
FIG. 3. Upper panel: Suppressed diffraction bright-field TEM image (taken at 150 kV), showing the mass and thickness contrast of $In_xGa_{1-x}As$ QDs on a GaAs surface. The image was obtained at a position on the wafer that corresponds to the largest amount of deposited $In_xGa_{1-x}As$ in Figs. 1 and 2.

aging, they were not covered. The sample location depicted in Fig. 3 corresponds to the PL and capacitance spectroscopies position with the largest $In_xGa_{1-x}As$ coverage. We therefore expect to see both sets of QDs. The histograms in Fig. 4 show that the distributions of the QD areas and heights are indeed bimodal. To be sure that the bimodal distribution is not an artifact of the binning used for the histograms, the inset shows a height vs area plot for all of the QDs in the $(940 \text{ nm})^2$ area for which the histogram is shown. As expected for a bimodal distribution, the data fall into two sets. From the histogram, we found mean areas of 220 nm^2
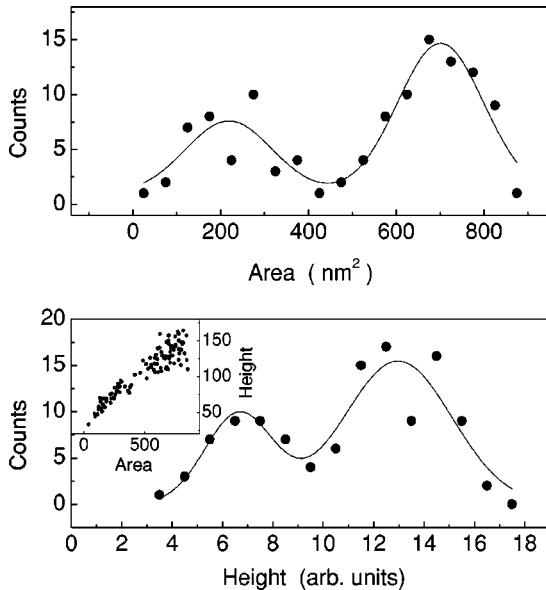

FIG. 4. Histograms of the area and height distribution of the QDs in Fig. 3. The lines are fits to a two-peak Gaussian. Inset: Height vs area for each of the QDs in the $(940 \text{ nm})^2$ area for which the histograms are shown.
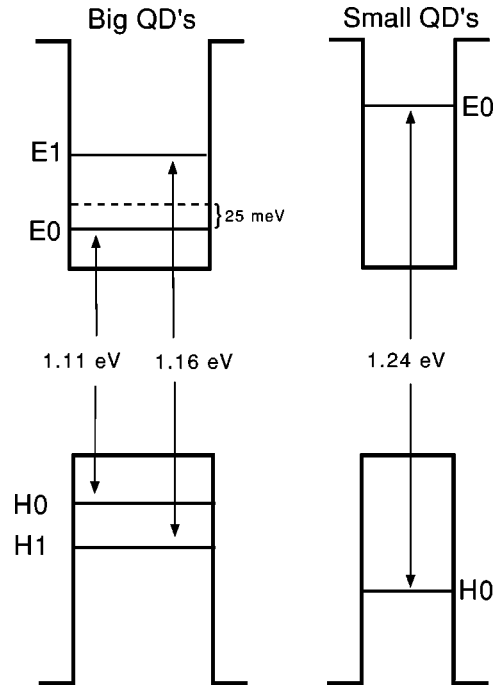

FIG. 5. Energy-level diagram of the big and small QDs, constructed from the PL and capacitance spectra of Figs. 1 and 2. See text for details.

and 700 nm^2. The height scale of the TEM data is not calibrated; from AFM measurements, we estimate that the distribution of heights peaks at 6.5 ± 1 nm and 12 ± 1 nm.

After having confirmed that a bimodal QD distribution is responsible for the two sets of observed signals, we now proceed to construct the energy-level diagram for the two kinds of QDs (Fig. 5). The first two peaks of the capacitance data in Fig. 1 correspond to the ground state of the big QDs, which appears split because of the Coulomb blockade. The second electron that tunnels into the QD needs to overcome the Coulomb-blockade energy of 25 meV. Because the QDs stay neutral during the PL measurements, Coulomb blockade was not observed in the PL data (Fig. 2). The third peak in the capacitance, at 115 meV, is probably caused by both types of QDs. AFM images show that with increasing $In_xGa_{1-x}As$ coverage, the number of small QDs decreases as more big QDs assemble. If the peak at 115 meV was caused only by small QDs, its amplitude would then depend on the position of the sample. We can obtain a consistent picture by assuming that at about 115 meV we observe not only the energy level of the ground state of the small QDs, but also the energy level of the first excited state of the big QDs. This rather wide third peak in the capacitance likely corresponds to the peaks at 1.16 eV and 1.24 eV in the PL data. Note that even though the capacitance features of the ground state of the small QDs and of the first excited state of the big QDs are superimposed as one wide maximum, they are well-separated in the PL data and in the energy-level diagram (Fig. 5). This is because the Coulomb-blockade splitting shifted the tunneling energies for the capacitance spectroscopy progressively upwards, while the detected PL features correspond to the "true" energies.[29]
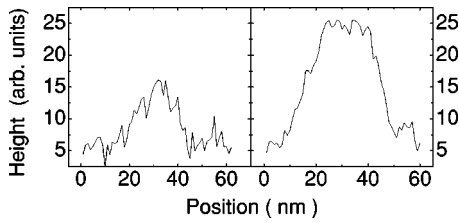
FIG. 6. Intensity cross sections of a small and a big QD from the TEM image in Fig. 3.

FIG. 7. Cross-sectional TEM image taken along the [110] zone of a small and a big QD.

There is another interesting point related to the fact that the amplitude of the capacitance feature at 115 meV is almost independent of the $In_xGa_{1-x}As$ coverage. AFM images find that the total number of QDs is almost independent of position. The total number of states that are filled at around 115 meV should vary nevertheless, because the first excited state is four-fold occupied for oblate nearly circular QDs, whereas the ground state is only two-fold occupied. This might explain why the traces at 115 meV did not fall exactly on top of each other.

To check whether the two QD sizes that are observed with TEM (Fig. 4) could indeed explain PL ground-state transmission energies that are separated by 0.13 eV (Fig. 2), we calculated the transition energy between electron and hole ground states for QDs with heights of 6.5 nm and 12 nm (obtained from AFM), and areas of 220 nm² and 700 nm² (obtained from TEM). To represent the QDs in our calculations, we used the effective-mass approximation and assumed that the small and big QDs are cylindrically symmetric cones. The effective-mass Schrödinger equation was solved using a mode-matching method to obtain the ground states of electrons and holes in the QDs. From this, we obtained PL ground-state emission energies of 1.111 eV and 1.254 eV for the large and small QDs, respectively. The energies are in good agreement with 1.11 eV and 1.24 eV, the emission energies obtained from PL.

Having established that a bimodal QD size distribution can account for the observed PL and capacitance energies, we next discuss the shape of the QDs and its possible influence on their In concentration. From the area and height histograms (Fig. 4) together with AFM data, we found that the aspect ratio of the small QDs, $2\sqrt{220}$ nm/$6.5\sqrt{\pi}$ nm $=2.57$, is similar to the aspect ratio of the large QDs, $2\sqrt{700}$ nm/$12\sqrt{\pi}$ nm$=2.49$. This does not necessarily imply that the QDs have the same shapes. Figure 6 shows the intensity profiles of the plan-view TEM image (Fig. 3). These profiles suggest that the small QDs have the shape of pyramids, whereas the big QDs—to minimize the strain energy—appear to be truncated pyramids with relatively flat tops. It should be noted, however, that the intensity profiles may not show the exact shape due to contributions to the overall contrast that may arise from residual diffraction and defocus effects, and the possibility of a nonuniform QD composition. Cross-sectional high-resolution TEM was performed along the [110] zone as a double check on the QD shape, and typical results are shown in Fig. 7. The results support the line profiles obtained from the plan-view TEM. The big QDs are truncated pyramids, with the steepest sec-
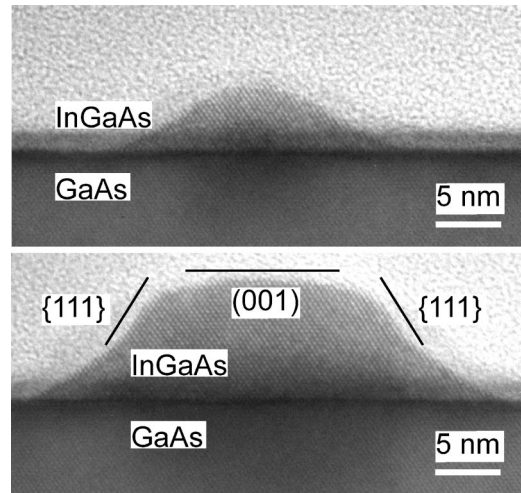
tions of the sides forming {111} facets while the tops are slightly domed. The cross-sectional TEM images also suggest that the small QDs have the shape of pyramids with less-steep side facets. In cross-sectional TEM it is difficult to distinguish between small QDs and large QDs that have been sectioned off center. However, we observed many QDS with the regular pyramid shape and statistically these could not all be big QDs sectioned off center. The excellent correlation between the QD shapes observed by cross-sectional TEM and the plan-view TEM suppressed diffraction technique suggests that the latter may be a reliable way to distinguish between different QD shapes. This is particularly so in the case of the small quantum dots since it avoids the possible confusion of small QDs with big QDs sectioned off center in TEM cross-section studies.

The shape differences we observed may influence the distribution of In in the QDs since In segregates toward the top of the QDs to minimize strain.[30] Since the truncated pyramids have a larger top area, it is conceivable that the big QDs contain a higher concentration of In. This would lower the energy levels of the big QDs and further enhance the energetic difference between big and small QDs.

An important open question is whether a bimodal QD size and shape distribution occurs in equilibrium, as proposed for the Ge/Si QD system[31] or if the size and shape depend on kinetic factors such as the surface diffusivity or the deposition rate.[32,33] Since our study did not explore growth dynamics, we cannot directly address this question. It is nevertheless interesting to speculate about the effects of strain on a growing pyramid of $In_xGa_{1-x}As$ as a possible origin of the bimodal size and shape distribution. We suggest that there is a maximum QD size that is consistent with a regular pyramidal shape.[34] Pyramids with a larger base would experience too much strain and break up into incoherent QDs, which are not favored at an early growth stage because of the interfacial energy between grains. However, $In_xGa_{1-x}As$ may still adhere to the top of the pyramid,[16,19,35] where the strain is partially relaxed and the lattice constant approaches that of bulk $In_xGa_{1-x}As$. These QDs may take on the shape of trun-

cated pyramids. Based on these assumptions, a bimodal QD distribution in size and shape forms when the amount of deposited $In_xGa_{1-x}As$ exceeds a critical thickness that depends on the dynamic conditions under which the QDs are grown. If the deposited In and Ga atoms are not given sufficient time to diffuse across the wafer's surface (by either increasing the deposition rate or decreasing the deposition temperature), their mean size will be smaller.[9,25] Maximum-sized regular pyramids, and therefore the conditions for a bimodal size and shape distribution, will be reached at a larger amount of deposited $In_xGa_{1-x}As$. This may be the reason why some other studies have not reported a bimodal QD size distribution of $In_xGa_{1-x}As$ or InAs QDs.[22,36,37]

In conclusion, we have analyzed the size distribution of self-assembled $In_xGa_{1-x}As$ quantum dots with capacitance and photoluminescence spectroscopies, and with TEM and AFM imaging. The observed spectroscopic signals can be separated into two distinct sets, which are shown by TEM and AFM to be caused by a bimodal QD size distribution. In addition, we find that the big and the small quantum dots have different shapes, which may further increase the difference between their energy levels. We suggest that the bimodal size and shape distribution may originate from the effect of strain on the growth of $In_xGa_{1-x}As$ pyramids on a GaAs surface. With the assumption that the ground-state capacitance peaks of the small quantum dots overlap with the first excited-state capacitance peaks of the big quantum dots, we can provide a consistent picture of the energy levels in both types of quantum dots.

[1] D. Bimberg, N. N. Ledentsov, N. Grundmann *et al.*, Phys. Status Solidi B **194**, 159 (1996).

[2] N. Kirstaedter, O. G. Schmidt, N. N. Ledentsov *et al.*, Appl. Phys. Lett. **69**, 1226 (1996).

[3] G. Yusa and H. Sakaki, Appl. Phys. Lett. **70**, 345 (1997).

[4] T. Lundstrom, W. Schoenfeld, H. Lee *et al.*, Science **286**, 312 (1999).

[5] A. Wojs and P. Hawrylak, Phys. Rev. B **55**, 13066 (1997).

[6] O. Stier, M. Grundmann, and D. Bimberg, Phys. Rev. B **59**, 5688 (1999).

[7] J. Drucker, Phys. Rev. B **48**, 18203 (1993).

[8] J. M. Garcia, G. Medeiros-Ribeiro, K. Schmidt *et al.*, Appl. Phys. Lett. **71**, 2014 (1997).

[9] P. B. Joyce, T. J. Krzyzewski, G. R. Bell *et al.*, Phys. Rev. B **62**, 10 891 (2000).

[10] F. Patella, M. Fanfoni, F. Arciprete *et al.*, Appl. Phys. Lett. **78**, 320 (2001).

[11] L. Brusaferri, S. Sanguinatti, E. Grilli *et al.*, Appl. Phys. Lett. **69**, 3354 (1996).

[12] G. G. Tarasov, Yu. I. Mazur, Z. Ya. Zhuchenko *et al.*, J. Appl. Phys. **88**, 7162 (2000).

[13] D. Leonard, K. Pond, and P. M. Petroff, Phys. Rev. B **50**, 11 687 (1994).

[14] R. P. Mirin, K. L. Silverman, D. H. Christensen *et al.*, J. Vac. Sci. Technol. B **18**, 1510 (2000).

[15] H. Y. Liu, B. Xu, Y. H. Chen *et al.*, J. Appl. Phys. **88**, 5433 (2000).

[16] Qianghua Xie, J. L. Brown, R. L. Jones *et al.*, J. Electron. Mater. **28**, L42 (1999).

[17] Qianghua Xie, J. L. Brown, and J. E. van Nostrand, Appl. Phys. Lett. **78**, 2491 (2001).

[18] S. P. Guo, A. Shen, Y. Ohno *et al.*, Physica E (Amsterdam) **2**, 672 (1998).

[19] I. Mukhametzhanov, Z. Wei, R. Heitz *et al.*, Appl. Phys. Lett. **75**, 85 (1999).

[20] K. H. Schmidt, G. Medeiros-Ribeiro, U. Kunze *et al.*, J. Appl. Phys. **84**, 4268 (1998).

[21] G. Medeiros-Ribeiro, D. Leonard, and P. M. Petroff, Appl. Phys. Lett. **66**, 1767 (1995).

[22] K. H. Schmidt, G. Medeiros-Ribeiro, J. Garcia *et al.*, Appl. Phys. Lett. **70**, 1727 (1997).

[23] H. Saito, K. Nishi, and S. Sugou, Appl. Phys. Lett. **73**, 2742 (1998).

[24] R. Leon, S. Fafard, P. G. Piva *et al.*, Phys. Rev. B **58**, R4262 (1998).

[25] L. Chu, M. Arzberger, G. Boehm *et al.*, J. Appl. Phys. **85**, 2355 (1999).

[26] J. Kim, L.-W. Wang, and A. Zunger, Phys. Rev. B **57**, R9408 (1998).

[27] M. Grassi Alessi, M. Capizzi, A. S. Bhatti *et al.*, Phys. Rev. B **59**, 7620 (1999).

[28] C.-P. Liu, P. D. Miller, W. L. Henstrom *et al.*, J. Microsc. **199**, 130 (2000).

[29] K. H. Schmidt, G. Medeiros-Ribeiro, M. Oestreich *et al.*, Phys. Rev. B **54**, 11 346 (1996).

[30] I. Kegel, T. H. Metzger, A. Lorke *et al.*, Phys. Rev. Lett. **85**, 1694 (2000).

[31] G. Medeiros-Ribeiro, A. M. Bratkovski, T. I. Kamins, D. A. Ohlberg, and R. S. Williams, Science **279**, 353 (1998).

[32] F. M. Ross, J. Tersoff, and R. M. Tromp, Phys. Rev. Lett. **80**, 984 (1998).

[33] F. M. Ross, R. M. Tromp, and M. C. Reuter, Science **286**, 1931 (1999).

[34] D. E. Jesson, G. Chen, K. M. Chen *et al.*, Phys. Rev. Lett. **80**, 5156 (1998).

[35] H. Saito, K. Nishi, and S. Sugou, Appl. Phys. Lett. **74**, 1224 (1999).

[36] R. Leon and S. Fafard, Phys. Rev. B **58**, R1726 (1998).

[37] S. Fafard, Z. R. Wasilewski, and M. Spanner, Appl. Phys. Lett. **75**, 1866 (1999).